Research Article

Enhanced electrochemical and photovoltaic performance for MoO_3 nanorods at different calcination temperature based counter electrode in Pt-free dye-sensitized solar cells applications

K. B. Bhojanaa[1,2] · S. Kannadhasan[3] · N. Santhosh[3] · P. Vijayakumar[4] · M. Senthil Pandian[3] · P. Ramasamy[3] · A. Pandikumar[1,2]

Received: 25 February 2020 / Accepted: 17 September 2020 / Published online: 30 September 2020

Abstract
Owing to increase in energy demands and depletion in fossil fuels, solar energy conversion is the reliable and sustainable one for future. Among the solar energy conversion techniques, dye-sensitized solar cells (DSSC) have received much attention due to their ease of fabrication, cost-effectiveness, reliable and high proficiency in converting solar energy. The commercialization of DSSC is still hindered by usage of expensive materials like platinum counter electrodes. Therefore, researchers are focusing on developing low-cost and earth abundant alternatives. The present work involves hydrothermal synthesis of molybdenum trioxide (MoO_3) at various temperature ranges such as 400, 500, 600 and 700 °C and several other characterizations through various analytical techniques. On increasing the temperature range, the MoO_3 forms nanorod like structure. The synthesized materials are employed as counter electrode in DSSC, showed enhanced power conversion efficiency (PCE) on increasing the calcination temperature range. The maximum PCE of 4.13% is obtained for MoO_3 calcined at 600 °C, which is highly comparable with the high cost platinum CE based DSSC.

Keywords Solar energy · Dye sensitized solar cells · Counter electrode · Molybdenum trioxide · Power conversion efficiency

1 Introduction

Increasing global energy demands urges to develop an efficient technology that harvest energy resources with minimal environmental impacts. For this, renewable energy sources such as wind, solar, geothermal, hydroelectricity are alternative strategies to overcome the issues. Among them, solar energy has many advantages such as non-exhaust, earth abundant etc., [1–3]. To harvest the solar energy, solar cells have been developed, which converts solar energy into electrical energy directly. It involves the solar cells with first, second and third generation devices. Currently, third generation solar cells are the emerging field of research [4]. In that, dye sensitized solar cells (DSSCs) receive much attention due to their ease of fabrication and cheaper than other solar cells. Normally, DSSC consists of four components namely sensitizer, photoanode, electrolyte and counter electrode. When light is illuminated, the dye molecules (sensitizer) get excited and injects the electron into the conduction band of the semiconductor photoanode. The electron from the conduction band

K. B. Bhojanaa and S. Kannadhasan have contributed equally to this work.

✉ A. Pandikumar, pandikumarinbox@gmail.com | [1]Academy of Scientific and Innovative Research (AcSIR), Ghaziabad 201002, India. [2]Electro Organic and Materials Electrochemistry Division, CSIR-Central Electrochemical Research Institute, Karaikudi, Tamil Nadu 630003, India. [3]SSN Research Centre, Sri Sivasubramaniya Nadar College of Engineering, Chennai, Tamil Nadu 603110, India. [4]State Key Laboratory for Mechanical Behavior of Materials, Xi'an Jiaotong University, Xi'an 710049, China.

of semiconductor flows through the external circuit and reaches the counter electrode. Counter electrode transfers electrons from the external circuit to the electrolyte, where the electrolyte helps the redox reaction in dye-sensitized solar cells [5–7]. Currently, researchers are focusing to commercialize the DSSC. However, it is still hindered by using platinum like counter electrode, because of their low abundance and high cost. Thus, fabrication of CEs with other low-cost materials may bring down the production cost of the DSSCs. So far, Pt-nanocomposite, polymer based counter electrode and transition metal compounds including carbide, nitrides and oxides are explored as a potential candidate to substitute Pt due to their distinguishing features such as low cost, thermal stability, durability, high thermal and electrical conductivity and their catalytic behavior that resembles platinum [8–13]. On comparing with carbides and nitrides based counter electrodes, only fewer studies are reported for oxides based counter electrodes. In oxide based counter electrodes, various transition metal oxides are attempted to study as a counter electrode for DSSC [14–19]. Of these, molybdenum trioxide (MoO_3) is one of the renowned oxide material, commonly used for versatile applications such as in energy storage, catalysis, electrochromics, photochromics, thermochromics, display materials, sensors [20–26]. It also exhibits good electrocatalytic activity, hence it could be the potential candidate for CE in DSSC. In this work, MoO_3 was prepared by hydrothermal method and is subjected to calcination at 400, 500, 600 and 700 °C. The prepared MoO_3 were characterized by suitable physicochemical techniques. The calcinated MoO_3 samples are used to fabricate CE for DSSC, of which, MoO_3 obtained at 600 °C shows PCE of about 4.13%.

2 Materials and methods

2.1 Chemicals and reagents

Ammonium molybdate tetra-hydrate ($(NH_4)_6Mo_7O_{24}\cdot 4H_2O$) (Merck), ethylene glycol (Merck), ruthenizer 535-bis TBA (N719) (Solaronix), Iodolyte HI-30 (Solaronix), Titanium Tetrachloride (spectrochem) and fluorine doped tin oxide (FTO) transparent conducting electrode (7 Ω cm^{-1}) (Hind High Vacuum, India) were purchased and used.

2.2 Synthesis of molybdenum trioxide (MoO_3)

The MoO_3 was prepared as follows (Scheme 1). Initially, 18.5 g of ammonium molybdate tetra-hydrate was dissolved in 150 ml of ethylene glycol and then stirred for 2 h at room temperature to form a homogeneous mixture. Then, the above mixture was transferred to autoclave and heated at 150 °C for 10 h. After allowing the mixture to cool naturally, the product was centrifuged, washed with distilled water four times, following which the orange color precipitate was obtained. Then the mixture was dried for 10 h at 80 °C. This dried product was subjected to calcination at 400, 500, 600 and 700 °C. The resultant product was black in colour, labelled as 400-MoO_3, 500-MoO_3, 600-MoO_3 and 700-MoO_3.

2.3 Fabrication of dye sensitized solar cells

2.3.1 Preparation of photoanode

The TiO_2 colloidal paste was prepared and casted on the FTO electrode using doctor blade technique and calcinated at 500 °C. $TiCl_4$ Treatment was made on TiO_2 coated film and sintered at 500 °C for 30 min. Then, TiO_2 coated electrode was dipped into a 0.5×10^{-3} M

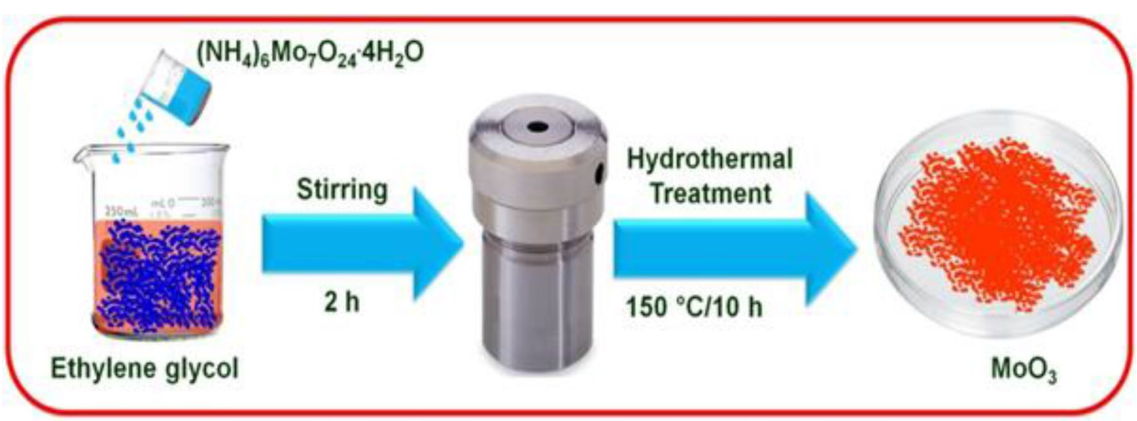

Scheme 1. Schematic representation of synthesis of MoO_3 nanorods

of photo-sensitizer (N719) containing acetonitrile and 4-tert-butanol (1:1) volume ratio for 24 h. The N719 attached TiO_2 electrode was rinsed with absolute ethanol to remove the unadsorbed dye and dried in N_2 flow for 30 min. Finally, the dye coated adsorbed photoanode was obtained.

2.3.2 Preparation of counter electrodes

The 400-MoO_3, 500-MoO_3, 600-MoO_3 and 700-MoO_3 modified CEs were fabricated by dispersing 50 mg of each material in ethanol and were sonicated until homogeneous colloidal suspensions is obtained. The resultant homogeneous colloidal suspensions were drop-casted on the FTO conducting surface and were dried at 120 °C for 24 h. Also, platinum coated FTO was prepared for the reference.

2.3.3 Assembly of dye-sensitized solar cells

The fabricated photoanode and CEs is dispensed with an aid of 100 µm thick surlyn spacer. Adequate amount of liquid electrolyte is applied over the dye sensitized TiO_2 film. Over this film, 400-MoO_3, 500-MoO_3, 600-MoO_3 and 700-MoO_3 platinum based CEs were placed. Finally, the DSSC was sandwiched using a clip. Before current density–voltage (J–V) measurement, the cell is masked using 5 mm × 5 mm non absorbing light black colour insulating tape.

2.3.4 Characterization techniques

The crystalline property of MoO_3 was analysed using a Rigaku powder X-ray diffractometer with Cu Kα (λ¼1.5406 Å) radiation over Bragg angle 2θ ranging within 10° to 80°. The morphological studies were carried out by a FESEM (Field Emission Scanning Electron Microscopy) and HRTEM (High-Resolution Transmission Electron Microscopy) (Carl Zeiss SIGMA field). The photovoltaic performance of the DSSC was evaluated using a Xenon lamp with a light intensity of 100 Mw cm^{-2} and an integrated air mass (AM) 1.5 G filter (ScienceTech, Canada). The J–V curves were measured using a Keithley Model 2400 multisource meter. Cyclic voltammetry (CV) and Electrochemical Impedance Spectra (EIS) analysis were performed with a computer-controlled potentiostat equipped with a frequency response analyzer (VERSASTAT 3-200).

3 Results and discussion

3.1 XRD characterization of the synthesized materials

The crystalline properties of synthesized materials were studied by PXRD pattern and are shown in Fig. 1. One can observe that on increasing the annealing temperature from 400 to 700 °C, the crystallinity of the material gets increased. For 600-MoO_3, the XRD pattern shows strong diffraction peaks at 2θ values of 13.25°, 23.75°, 26.15°, 27.72°, 39.35°, 46.64°, and 58.05°, which correspond to (001), (101), (002), (011), (112), (013) and (014) crystal planes of monoclinic MoO_3 (JCPDS NO. 47-1320) and cell parameters, a = 3.954 Å, b = 3.687 Å, c = 7.095 Å and d = 103.75° [27]. A high intense characteristic peak is observed at 26.15° (Fig. 1c); confirming the (002) plane of monoclinic MoO_3. This confirms a high crystalline behavior of MoO_3. In addition, the intensities of the 600-MoO_3 material is stronger at higher temperature, revealing that the 600-MoO_3 possess high preferential orientation along with the [002] direction to the nanorod structure. When the temperature increased to 700 °C the crystal phase changes to α-MoO_3 orthorhombic phase with a zone axis along the (010) direction. This implies that preferential growth occurred along the c-axis or (001) direction, implying that high degree of crystallinity.

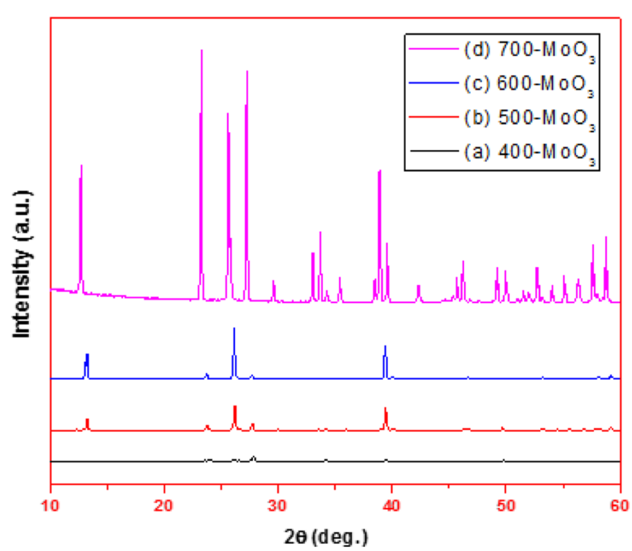

Fig.1 XRD patterns of (*a*) 400-MoO_3, (*b*) 500-MoO_3, (*c*) 600-MoO_3 and (*d*) 700-MoO_3

3.2 Morphological studies

The morphology of the synthesized MoO_3 powders were examined with scanning electron microscopy (SEM). The SEM images of MoO_3 powders are shown in Fig. 2a–h. From the SEM image all the four samples shows rod like structure. The crystallinity of the material increases with the annealing temperature as clearly perceived from the SEM images of 400-MoO_3, 500-MoO_3, 600-MoO_3 and 700-MoO_3. For 400-MoO_3, still unreacted MoO_2 precursors are present and hence there is no formation of nanorod.

Moreover, as evidenced from SEM images of 400-MoO_3, 500-MoO_3 samples consists of a greater number of aggregations formed from MoO_2 precursors. But for 500-MoO_3, the formation of nanorods began, and it is achieved at 600-MoO_3. The formation of nanorods improves with the reaction temperature, especially in the sample calcinated at 600 °C, where a large number of nanorods can be observed. Further increasing the annealing temperature to 700 °C a well crystalline microrod like structure occurred. The distribution density of the nanorods increases with the calcination temperature as well. For deeper understanding about the morphology of 600-MoO_3, it is subjected to TEM analysis. Figure 3 shows (a) TEM image and (b) spot pattern of 600-MoO_3 respectively. From the TEM image of 600-MoO_3, the particle size of 600-MoO_3 is found to be 200 nm. The 'd' value obtained from the spot pattern of 600-MoO_3 is matched well with the 'd' value obtained from XRD.

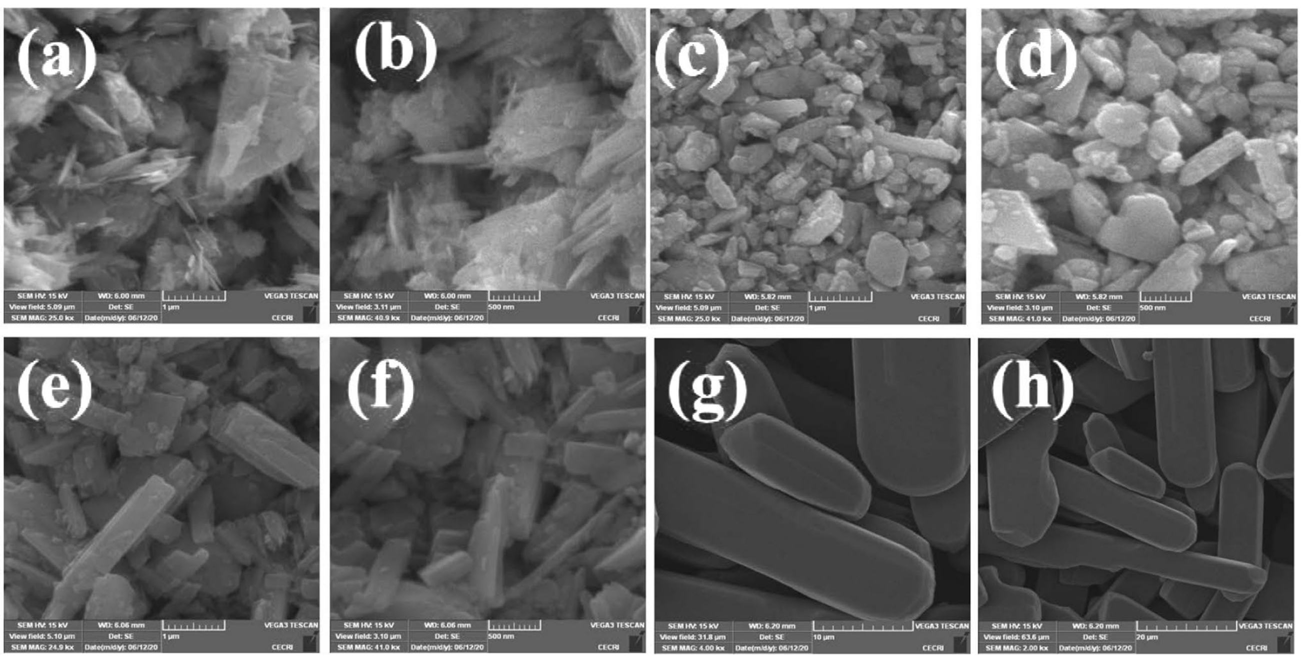

Fig.2 SEM images of **a**, **b** 400-MoO_3, **c**, **d** 500-MoO_3, **e**, **f** 600-MoO_3 and **g**, **h** 700-MoO_3

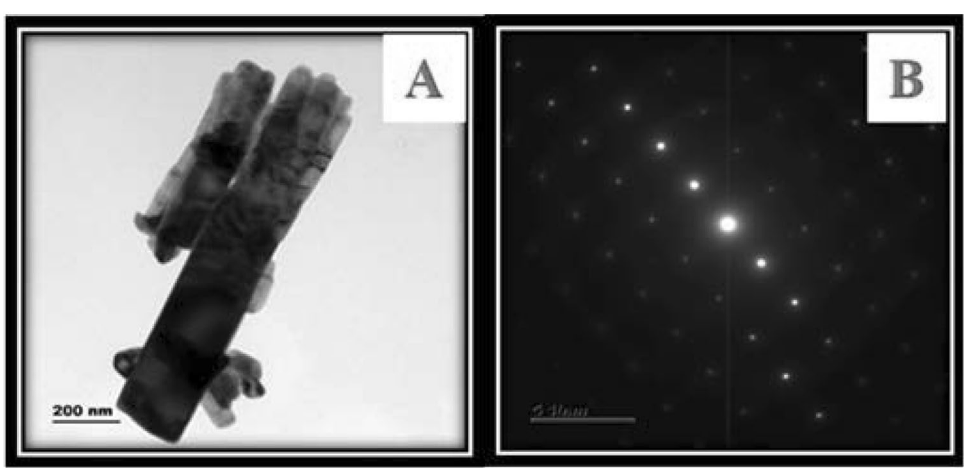

Fig.3 TEM image of **a** 600-MoO_3 and **b** Spot pattern of 600-MoO_3

Fig.4 Schematic illustration of DSSC mechanism

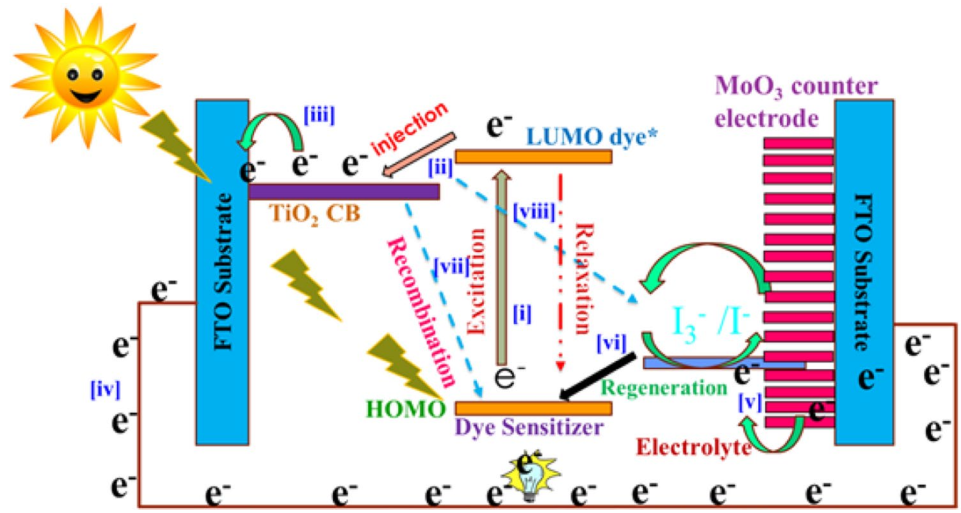

3.3 Photovoltaic performance of DSSC with different MoO_3 materials

Under sun light illumination, a dye molecule sensitized from HOMO to LUMO energy level (1) and the excited electron injects into the conduction band of TiO_2 (2), the dye molecule becomes oxidized. The injected electron is transported in between the TiO_2 nanoparticles and then extracts through the FTO substrate (3) and external circuit (4), and reaches the counter electrode. The electrolyte contains I^-/I_3^- redox ion, this is used as mediator between TiO_2 photoanode and counter electrode. The electrolyte is regenerating the oxidized dye molecule (5) and reduced by electron from counter electrode (6). The electron transfer process is hindered by electron recombination. (a) The injected electrons are recombining between conduction band of TiO_2 and sensitized hole (7). (b) Another recombination process occurs between conduction band of TiO_2 and oxidation of redox couple (8). This recombination process reduces the performance of DSSC devices [28–30] (Fig. 4).

The photovoltaic performances of the (a) 400-MoO_3, (b) 500-MoO_3, (c) 600-MoO_3 (d) 700-MoO_3 and (e) Platinum based DSSCs were investigated under a simulated solar irradiation of 100 mWcm^{-2} (AM 1.5 G) and their photocurrent density–photovoltage (J–V) curve is shown in Fig. 5. The corresponding photovoltaic parameters are listed in Table 1. Short-circuit photocurrent density (Jsc) obtained for (a) 400-MoO_3, (b) 500-MoO_3, (c) 600-MoO_3 (d) 700-MoO_3 and (e) Platinum based DSSCs are 6.308, 6.876, 9.448, 7.012 and 9.126 mA cm^{-2} respectively. Open-circuit photovoltage (Voc) obtained for (a) 400-MoO_3, (b) 500-MoO_3, (c) 600-MoO_3 (d) 700-MoO_3 and (e) Platinum based DSSCs are 0.717, 0.726, 0.70, 0.68 and 0.72 V, respectively with the fill factor of 0.658, 0.622, 0.625, 0.579 and 0.658. The efficiency of (a) 400-MoO_3, (b) 500-MoO_3, (c) 600-MoO_3

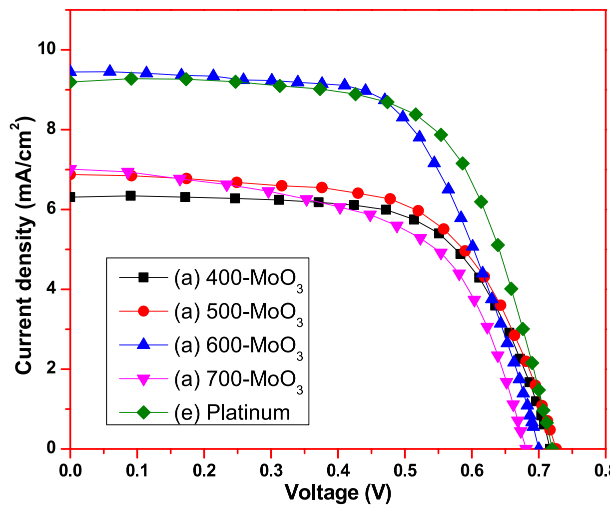

Fig.5 Current density–voltage (J–V) curves obtained for (*a*) 400-MoO_3, (*b*) 500-MoO_3, (*c*) 600-MoO_3 (*d*) 700-MoO_3 and (*e*) platinum based DSSCs sensitized with N719 dye under simulated AM 1.5 G solar irradiation of 100 mW cm^{-2}

Table 1 Photovoltaic parameters derived for different MoO_3 modified and Pt based CE in DSSCs

Counter electrode	J_{sc} (mA cm^{-2})	V_{oc} (V)	FF	η (%)
400-MoO_3	6.308	0.717	0.658	2.98
500-MoO_3	6.876	0.726	0.622	3.1
600-MoO_3	9.448	0.7	0.625	4.13
700-MoO_3	7.012	0.68	0.579	2.76
Platinum	9.192	0.72	0.658	4.35

The DSSCs performance was evaluated under 100 mW cm^{-2} simulated AM 1.5 G solar light irradiation. J_{sc}: Short-circuit current density; V_{oc}: Open-circuit voltage; FF: Fill factor; η: Power conversion efficiency. Area of the cell was 0.25 cm^2.

(d) 700-MoO_3 and (e) Platinum are 2.98, 3.1, 4.13, 2.76 and 4.35% respectively. It can be clearly seen that the efficiency increased with increasing the calcination temperatures and their crystalline nature. On comparing the platinum based counter electrode 600-MoO_3 based counter electrode material, showed comparable efficiency. From this, the catalytic behavior of the 600-MoO_3 is revealed. Hence, 600-MoO_3 could be the better alternative to the platinum counter electrode.

3.4 Cyclic voltammetry analysis

Cyclic voltammetry (CV) is an important tool to investigate the electrocatalytic behaviors of different electrodes toward the reduction of triiodide. The cyclic voltammetric (CV) technique was carried out in a three electrode system namely, working, counter and reference electrodes. The FTO coated with 400-MoO_3, 500-MoO_3, 600-MoO_3 and platinum are employed as a working electrode and subjected to CV analysis at a scanning rate of 50 mV s^{-1}. The crucial operation of CE in DSSC is reducing the triiodide ions, therefore the reduction peak current density of left side peak is generally identified as the characteristic of superior catalytic ability [26]. Figure 6 shows the CV curves of (a) 400-MoO_3, (b) 500-MoO_3, (c) 600-MoO_3 and (d) Platinum based CEs. In this figure, the left side redox pair represents the electrocatalytic reduction of I_3^- to I^- that is $I_3^- + 2e^- \rightarrow 3I^-$, causes the cathodic current (I_{Pc}). The cathodic current density (I_{Pc}) of (a) 400-MoO_3, (b) 500-MoO_3, (c) 600-MoO_3 and (d) Platinum are 6.5897×10^{-4}, 4.7722×10^{-4}, 11.4500×10^{-4} and 19.702×10^{-4} $mAcm^{-2}$, respectively. Higher the I_{Pc} value, greater would be the catalytic activity [31].

It is clearly seen that, among the synthesized materials, 600-MoO_3 shows maximum current density than 400-MoO_3 and 500-MoO_3. The peak-to-peak separation (E_{PP}) got decreased on moving from 400-MoO_3 and 500-MoO_3, to 600-MoO_3. Increased I_{Pc} value and decreased E_{PP} value, reveals the better catalytic behaviour of 600-MoO_3. Thus, on increasing the calcination temperature, the active sites of the material gets increased and hence results in better catalytic activity.

3.5 Electrochemical impedance analysis

To investigate the charge-transfer characteristics of various CEs on the electrode/electrolyte interface, EIS analysis are performed on the symmetric cells consisting two identical electrodes. To carry out EIS experiments, symmetric cell was constructed with 400-MoO_3, 500-MoO_3, 600-MoO_3 and Platinum CEs. It is employed to analyse the interfacial charge transfer process and electrocatalytic activity of DSSC. Figures 7 and 8 represents EIS studies of (a) 400-MoO_3, (b) 500-MoO_3, (c) 600-MoO_3 and (d) Platinum CEs by Nyquist and Bode plots and these parameters are shown in Table 2.

In the Nyquist plots, the intercept in the high frequency region on the X-axis determines the series resistance (R_s) of the device, which generates from contact resistance and sheet resistance. The first and second semicircle describes about the charge-transfer processes at the CE/electrolyte interface and TiO_2/dye/electrolyte interface respectively, of the DSSC. The third curve represents the Warburg diffusion process of I^-/I_3^- in the electrolyte [32, 33]. The R_S (Series resistance) values obtained for 400-MoO_3, 500-MoO_3, 600-MoO_3 and platinum are 6.6074, 10.8767,

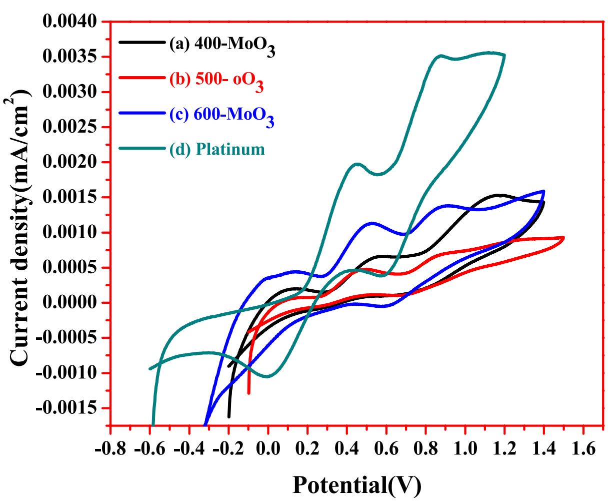

Fig.6 Cyclic voltammograms obtained for (*a*) 400-MoO_3, (*b*) 500-MoO_3, (*c*) 600-MoO_3 and (*d*) Platinum based counter electrodes at a scanning rate of 50 mV s^{-1}

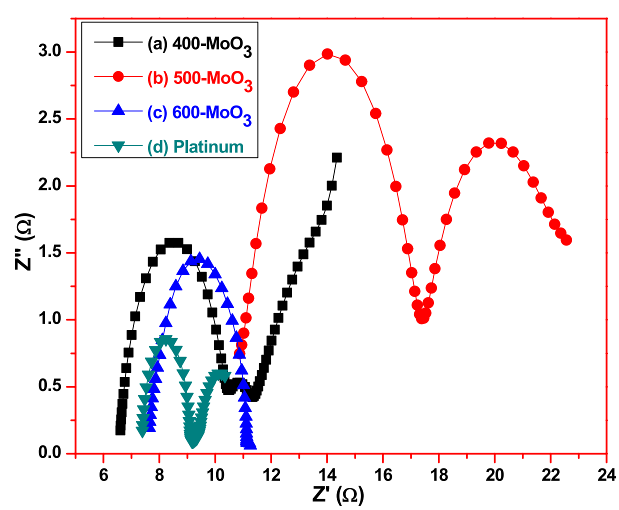

Fig.7 Nyquist plot obtained for (*a*) 400-MoO_3, (*b*) 500-MoO_3, (*c*) 600-MoO_3 and (*d*) Platinum based counter electrodes of dye sensitized solar cells

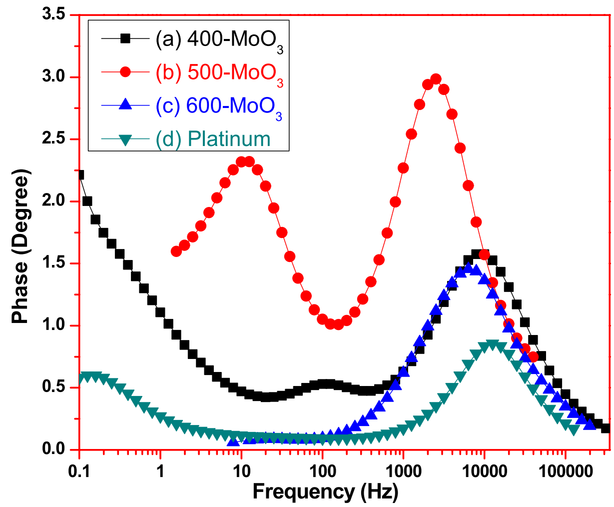

Fig.8 Bode plots obtained for (*a*) 400-MoO_3, (*b*) 500-MoO_3, (*c*) 600-MoO_3 and (*d*) Platinum based counter electrodes of dye sensitized solar cells

7.6388 and 7.3930 Ω cm^2 respectively. The smaller R_s values indicated the good bonding strength between FTO and coated counter electrode material. It is seen that, in Fig. 7 the charge transfer resistance (R_{ct1}) values for 400-MoO_3, 500-MoO_3 600-MoO_3 and Platinum are 10.51, 17.46, 11.2542 and 9.1961 Ω cm^2 respectively.

As the other catalytic information of EIS measurement, Bode-phase plot can provide the electron lifetime (τ). The lower electron lifetime indicating that electrons from external circuit are quickly transferred to the electrolyte for regenerating I^- ions, i.e. the electrode holds superior catalytic ability. Figure 8 shows the Bode phase plots obtained for 400-MoO_3, 500-MoO_3, 600-MoO_3 and Platinum CEs based DSSCs. The maximum frequency of the characteristic frequency peak obtained from the bode phase plots for 400-MoO_3, 500-MoO_3, 600-MoO_3 and Platinum are 7943.282, 2511.886, 6309.573 and 12,589.25 Hz respectively. The electron lifetime was calculated from the following equation.

$$\tau_n = \frac{1}{2\pi f_{max}}$$

where f_{max} is the maximum frequency of the characteristic frequency peak from Bode phase plot [26].

Their corresponding calculated electron lifetime (τ_n) are 20.042, 63.379, 25.232 and 12.646 μs. It can be seen that the 600-MoO_3 based CE shows shorter lifetime due to the rapid electron transfer process thus cause the DSSC performs better.

4 Conclusion

In this study, the MoO_3 nanorods were prepared by simple hydrothermal method using ammonium molybdate as precursor. The prepared MoO_3 nanorods were calcinated at 400, 500, 600 and 700 °C. The XRD results reveal the crystalline nature of MoO_3 samples and crystal phase of MoO_3 changes when exceeding the sintering temperature at 600 °C. The SEM and HRTEM studies confirm the nanorods morphology of MoO_3. The prepared 600-MoO_3 used as counter electrode in DSSC and shows 4.35% power conversion efficiency which is more on comparing with Pt based CE DSSCs (4.13%). The results reveal that calcination temperatures influence the photovoltaic parameters due to the formation of nanorod structure that alter the catalytic performance of 600-MoO_3. Further EIS data supports the best counter electrode behaviour of 600-MoO_3 due to less charge transfer resistance. Thus, the hydrothermally prepared MoO_3 nanorods could be a cheap and efficient counter electrode material which is alternative to expensive Pt counter electrode based DSSCs.

Table 2 Electrochemical parameters obtained for different MoO_3 modified and Pt based CE in DSSCs

Counter electrode	R_s (Ω cm^2)	R_{ct1} (Ω cm^2)	$\lvert I_{pc}\rvert$ (mA cm^{-2})	$\lvert E_{PP}\rvert$ (V)	τ_n (μs)
400-MoO_3	6.61	10.51	0.55	0.27	20.042
500-MoO_3	10.88	17.46	0.47	0.18	63.379
600-MoO_3	7.64	11.25	0.50	0.08	25.232
Platinum	7.39	9.20	0.45	0.44	12.646

The electrochemical impedance spectra (EIS) were recorded in the frequency range of 0.01 Hz to 100 kHz. R_s: the sheet resistance of transparent conductive oxide (TCO) and Pt counter electrode and the resistance of the electrolyte; R_{ct1}: Charge transfer resistance at counter electrode and electrolyte interface; cathodic current density (I_{pc}); peak-to-peak separation (Epp); τ_n: Electron life-time.

Acknowledgements The authors are grateful to DST-SERI (DST/TMD/SERI/S76(G)), the government of India, for financial support. Ms. K. B.Bhojanaa (IF170765) thanks DST for INSPIRE Fellowship.

Compliance with ethical standards

Conflicts of interest The Author declares no conflicts of interest.

References

1. Owusu PA, Asumadu-Sarkodie S (2016) A review of renewable energy sources, sustainability issues and climate change mitigation. Cogent Eng 3:1167990
2. Abbasi T, Premalatha M, Abbasi SA (2011) The return to renewables: Will it help in global warming control? Renew Sustain Energy Rev 15:891–894
3. Sharma S, Jain KK, Sharma A (2015) Solar cells: in research and applications—a review. Mater Sci Appl 6:1145
4. Ranabhat K, Patrikeev L, AevnaRevina A, Andrianov K, Lapshinsky V, Sofronova E (2016) An introduction to solar cell technology. J Appl Eng Sci 14:481–491
5. Anders H, Gerrit B, Licheng BS, Lars K, Henrik P (2010) Promoting effect of graphene on dye-sensitized solar cells. Chem Rev 110:6595–6663
6. Ye M, Wen X, Wang M, Iocozzia J, Zhang N, Lin C, Lin Z (2015) Recent advances in dye-sensitized solar cells: from photoanodes, sensitizers and electrolytes to counter electrodes. Mater Today 18:155–162
7. Sharifi N, Tajabadi F, Taghavinia N (2014) Recent developments in dye-sensitized solar cells. ChemPhysChem 15:3902–3927
8. Mozaffari S, Nateghi MR, Zarandi MB (2017) An overview of the challenges in the commercialization of dye sensitized solar cells. Renew Sustain Energy Rev 71:675–686
9. Calogero G, Calandra P, Irrera A, Sinopoli A, Citro I, Di Marco G (2011) A new type of transparent and low cost counter-electrode based on platinum nanoparticles for dye-sensitized solar cells. Energy Environ Sci 4:1838–1844
10. Regan BO, Grätzel M (1991) A low-cost, high-efficiency solar cell based on dye-sensitized colloidal TiO_2 films. Nature 353:737
11. Zhang L, Que L, Wu W, Wu J (2015) Preparation of Pt–NiO/Co_3O_4 nanocompounds based counter electrodes from Pt–Ni/Co alloys for high efficient dye-sensitized solar cells. J Alloy Compd 646:80–85
12. Zhang L, Wu J, Gao S, Lin J, Huang M, Chen X (2014) Template-free synthesis of polyaniline nanobelts as a catalytic counter electrode in dye-sensitized solar cells. Polym Adv Technol 25:343–346
13. Zhang L, Wu J, Lin J, Huang M, Wang X (2012) Enhancing photovoltaic performance of dye-sensitized solar cells by using thermally decomposed mirror-like Pt-counter electrodes. Thin Solid Films 522:425–429
14. Gao C, Han Q, Wu M (2018) Review on transition metal compounds based counter electrode for dye-sensitized solar cells. J Energy Chem 27:703–712
15. Wu J, Lan Z, Lin J, Huang M, Huang Y, Fan L, Luo G, Lin Y, Xie Y, Wei Y (2017) Counter electrodes in dye-sensitized solar cells. Chem Soc Rev 46:5975–6023
16. Hui W, Wei W, Yun H, Hu C (2014) J Mater Chem A 2:3065
17. Cui W, Ma J, Wu K, Chen J, Wu M (2017) The preparation and performance of W_3@C as a counter electrode catalyst for dye-sensitized solar cell. Int J Electrochem Sci 12:11487–11495
18. Lin X, Wu M, Wang Y, Hagfeldt A, Ma T (2011) Novel counter electrode catalysts of niobium oxides supersede Pt for dye-sensitized solar cells. Chem Commun 47:11489–11491
19. Zhou H, Shi Y, Dong Q, Wang Y, Zhu C, Wang L, Wang N, Wei Y, Tao S, Ma T (2014) Interlaced $W_{18}O_{49}$ nanofibers as a superior catalyst for the counter electrode of highly efficient dye-sensitized solar cells. J Mater Chem A 2:4347–4354
20. Tamboli PS, Prasad MBR, Kadam VS, Vhatkar RS, Pathan HM, Mahajan SS (2017) α-MoO_3-C composite as counter electrode for quantum dot sensitized solar cells. Sol Energy Mater Sol Cells 161:96–101
21. Cheng CK, Lin JY, Huang KC, Yeh TK, Hsieh CK (2017) Enhanced efficiency of dye-sensitized solar counter electrodes consisting of two-dimensional nanostructural molybdenum disulfide nanosheets supported Pt nanoparticles. Coatings 7:167
22. Sim K, Sung SJ, Jo HJ, Jeon DH, Kim DH, Kang JK (2013) Electrochemical investigation of high-performance dye-sensitized solar cells based on molybdenum for preparation of counter electrode. Int J Electrochem Sci 8:8272–8281
23. Ashok A, Vijayaraghavan SN, Nair SV, Shanmugam M (2017) Molybdenum trioxide thin film recombination barrier layers for dye sensitized solar cells. RSC Adv 7:48853–48860
24. Vijayakumar P, Senthil Pandian M, Lim SP, Pandikumar A, Huang NM, Mukhopadhyay S, Ramasamy P (2015) Facile synthesis of tungsten carbide nanorods and its application as counter electrode in dye sensitized solar cells. Mater Sci Semicond Process 39:292–299
25. Yan W, Ge W, Qian Y, Lin S, Zhou B, Liu WK, Lin F, Wagner GJ (2017) Multi-physics modeling of single/multiple-track defect mechanisms in electron beam selective melting. Acta Mater 134:324–333
26. Paranthaman V, Muthu SP, Alagarsamy P, Ming HN, Perumalsamy R (2016) Influence of zirconium dioxide and titanium dioxide binders on the photovoltaic performance of dye sensitized solar cell tungsten carbide nanorods based counter electrode. Electrochim Acta 211:375–384
27. Xu Y, Liu T, Li Y, Liu Y, Ge F (2018) Nanostructure design and catalytic performance of Mo/ZnAl-LDH in cationic orchid X-BL removal. Materials (Basel) 11:2390
28. van de Lagemaat J, Park N-G, Frank AJ (2000) Influence of electrical potential distribution, charge transport, and recombination on the photopotential and photocurrent conversion efficiency of dye-sensitized nanocrystalline TiO_2 solar cells: a study by electrical impedance and optical modulation techniques. J Phys Chem B 104:2044–2052
29. Bisquert J, Zaban A, Salvador P (2002) Analysis of the mechanisms of electron recombination in nanoporous TiO_2 dye-sensitized solar cells. Nonequilibrium steady-state statistics and interfacial electron transfer via surface states. J Phys Chem B 106:8774–8782
30. Wong W-Y, Ho C-L (2010) Organometallic photovoltaics: a new and versatile approach for harvesting solar energy using conjugated polymetallaynes. Acc Chem Res 43:1246–1256
31. Vijayakumar P, Senthil Pandian M, Pandikumar A, Ramasamy P (2017) A facile one-step synthesis and fabrication of hexagonal palladium-carbon nanocubes (H-Pd/C NCs) and their application as an efficient counter electrode for dye-sensitized solar cell (DSSC). Ceram Int 43:8466–8474
32. Vijayakumar P, Govindaraj R, Santhosh N, Pandian MS, Pandikumar A, Ramasamy P (2018) Investigation of suitable binder combination and electrochemical charge transfer dynamics of vanadium carbide nanoparticles-based counter electrode in Pt-free dye-sensitized solar cell. J Mater Sci 53:4444–4455

33. Lim SP, Pandikumar A, Lim YS, Huang NM, Lim HN (2014) In-situ electrochemically deposited polypyrrole nanoparticles incorporated reduced graphene oxide as an efficient counter electrode for platinum-free dye-sensitized solar cells. Sci Rep 4:5305